

An Artificial Neural Network Approach to Classification of Galaxy Spectra

S. R. Folkes,¹ O. Lahav¹ and S. J. Maddox²

¹ *Institute of Astronomy, The Observatories, Madingley Road, Cambridge, CB3 0HA*

² *Royal Greenwich Observatory, Madingley Road, Cambridge, CB3 0EZ*

Accepted Received

ABSTRACT

We present a method for automated classification of galaxies with low signal-to-noise (S/N) spectra typical of redshift surveys. We develop spectral simulations based on the parameters for the 2dF Galaxy Redshift Survey, and with these simulations we investigate the technique of Principal Component Analysis when applied specifically to spectra of low S/N. We relate the objective principal components to features in the spectra and use a small number of components to successfully reconstruct the underlying signal from the low quality spectra. Using the principal components as input, we train an Artificial Neural Network to classify the noisy simulated spectra into morphological classes, revealing the success of the classification against the observed b_J magnitude of the source, which we compare with alternative methods of classification. We find that more than 90% of our sample of normal galaxies are correctly classified into one of five broad morphological classes for simulations at $b_J=19.7$. By dividing the data into separate sets we show that a classification onto the Hubble sequence is only relevant for normal galaxies and that spectra with unusual features should be incorporated into a classification scheme based predominantly on their spectral signatures. We discuss how an Artificial Neural Network can be used to distinguish normal and unusual galaxy spectra, and discuss the possible application of these results to spectra from galaxy redshift surveys.

Key words: cosmology: miscellaneous - galaxies: classification - methods: data analysis

1 INTRODUCTION

In the near future new galaxy surveys will provide a large number of spectra, which will enable important measurements of galaxy properties. For example, the 2 degree field (hereafter 2dF) Galaxy Survey aims to collect 250,000 spectra. The integrated spectrum of a galaxy is a measure of its stellar composition and gas content, as well as its dynamical properties. Moreover, spectral properties often correlate fairly closely with galaxy morphology. Indeed, as the spectra are more directly related to the underlying astrophysics, they could prove a more robust classifier for evolutionary and environmental studies. Spectra can be obtained to larger redshifts than ground-based morphologies and, as 1-D data sets, are easier to analyse. Although the concept of spectral classification goes back to Humason (1936) and Morgan & Mayall (1957), few uniform data sets are available and a number of different approaches to the problem are possible.

Spectral classification is important for several practical and fundamental reasons. In order to derive luminosities corrected for the effects of redshift, the k -correction must be estimated for each galaxy. The rest-frame spectral energy dis-

tribution is needed, which can be obtained by matching the observed spectrum against templates of local galaxies. The proportion of sources in each class as a function of luminosity and redshift is of major interest. Apart from its relevance for environmental and evolutionary studies, new classes of objects may be discovered as outliers in spectral parameter space. Furthermore, by incorporating spectral features with other parameters (e.g. colour and velocity dispersion) an ‘H-R diagram for galaxies’ can be examined with possible important implications for theories of galaxy formation.

In this paper we explore the PCA and Artificial Neural Network (hereafter ANN) combination when applied to noisy galaxy spectra. PCA has been demonstrated to be a useful tool for spectral classification, with applications to stellar spectra (e.g. Murtagh & Heck 1987; von Hippel et al. 1994), QSO spectra (Francis et al. 1992) and galaxy spectra (Sodré & Cuevas 1994; Sodré & Cuevas 1996; Connolly et al. 1995). ANNs have been used for classification of images (Storrie-Lombardi et al. 1992; Naim et al. 1995; Lahav et al. 1995) and stellar spectra (Storrie-Lombardi et al. 1994) along with a variety of other astronomical applications. Other approaches have also been taken, such as

analysing the weight of specific components in each galaxy spectrum (Zaritsky et al. 1995). This approach is similar to the PCA technique, but the templates do not form an orthogonal set, although they can be chosen specifically to highlight certain characteristics in the spectra, such as young stars or emission lines. However, this approach does not allow for spectral variations extending outside the scope of the predetermined template set.

In this paper we use PCA on the complete spectra of the data set as opposed to some other spectral analyses which use specific measured quantities from the spectra (e.g. line strengths). We prefer to use the complete data so that we are not restricted to a set of predetermined measures. By using all the available data, the S/N inherent in the method is increased.

ANNs, originally suggested as simplified models of the human brain, are computer algorithms which provide a convenient general-purpose framework for classification (e.g. Hertz et al. 1991). ANNs are related to other statistical methods common in Astronomy and other fields. In particular ANNs generalize Bayesian methods, multi-parameter fitting, PCA, Wiener filtering and regularisation methods (e.g. Lahav et al. 1996).

We take the approach of using a fairly small set of high S/N spectra, and degrade them using the parameters of the 2dF system on the AAT. This produces simulated spectra for a range of possible noise levels which allows us to quantify the affect of the increasing noise and put limits on the success rates we hope to achieve for the spectral classification. In section 2 we describe the data set and show examples of the simulations. In section 3 we utilize the technique of Principal Component Analysis to compress the data set and to extract the ‘real’ information from the noisy spectra, leading to section 4, where we look at the spectral reconstructions based on the PCA, highlighting the ideal methods to use. In section 5 we use an Artificial Neural Network to operate on the results from the PCA, and demonstrate the level of classification success attained by this method. We end with a discussion of the results and the conclusions of the investigation.

2 DATA

The spectra used in this investigation are taken from the spectrophotometric atlas of galaxies (Kennicutt 1992) and represent the integrated spectra of local galaxies. They have been selected to demonstrate a wide range of spectral signatures. Most of the spectra have 5-8Å resolution but a few have been observed giving a lower resolution of 10-25Å. The spectra cover the wavelength range from 3650-7100Å, although for the purposes of this paper, we are left with a slightly shorter range when the simulation process has been applied (see Appendix A). More details of the observations are given in Kennicutt (1992). For the purposes of this paper the spectra have been split into two groups. The ‘Normal26’ spectra have been selected as being representative spectra for galaxies of normal morphological type, i.e. galaxies which conform simply to the Hubble classification scheme (Hubble 1936). The ‘Unusual29’ spectra comprise the remainder of the galaxies observed by Kennicutt. These spectra include peculiar and starburst galaxies and also galaxies with

Table 1. Morphological groups. Each group is given a name, a number G (for use in section 5), the T -Types covered by the group and the percentage of the galaxies in the ESO catalogue which fall into that group.

<i>Group</i>	G	T -Types	<i>ESO %</i>
E,S0	1	$T \leq 0.5$	21.0
Sa	2	$0.5 < T \leq 2.5$	16.9
Sb	3	$2.5 < T \leq 4.5$	20.9
Scd	4	$4.5 < T \leq 8.5$	30.1
Irr	5	$8.5 < T$	11.1

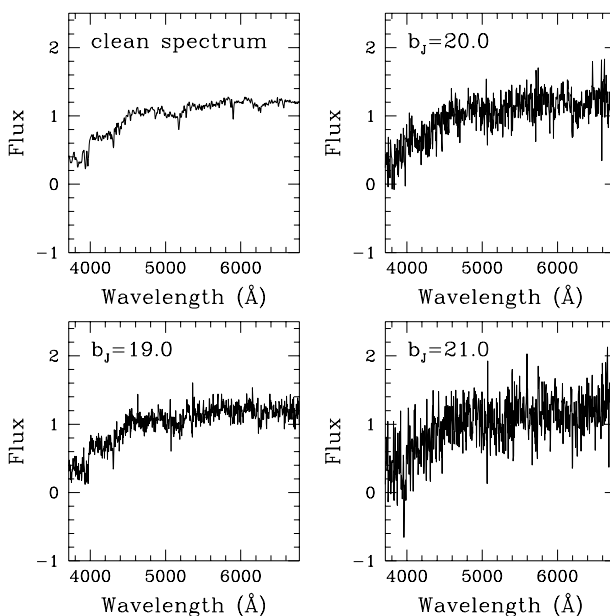


Figure 1. Simulated spectra based on NGC 3379 (E0).

Seyfert nuclei. The Normal26 spectra have been split into five broad groups, based on their visual morphology. These groups can be seen in Table 1 which also gives the percentage of galaxies falling into each group for the ESO catalogue (Lauberts & Valentijn 1989). We decided to bin the data in this way so that there are a number of spectra in each group and the ANN is not over-trained to recognize a specific spectrum for a particular class. With the small data set that we have, this is still a risk, but the combination of this binning and using many noisy deviates of each spectrum helps to alleviate the problem. Unfortunately the ‘Irr’ group is not well represented in the Normal26 sample, since all but two of these galaxies fall into the Unusual29 set. The Unusual29 spectra have also been tentatively placed in these 5 groups, based on their visual morphology where it is defined. Spectra without a defined morphology, or purely labeled as peculiar, have been placed in the final bin. Table 2 summarizes the data set. A notes section is also given for the Unusual29 spectra, which specifies why they have been categorized as unusual. Two of the spectra were found to adversely bias the PCA, and so have been removed from the normal set of spectra. In the case of NGC 1569 this is due to serious galactic reddening being evident in the continuum. In the case of MK 487 the reason is less obvious, but visual inspec-

Table 2. The selection of galaxy spectra from Kennicutt (1992).

Normal26			Unusual29			
<i>Galaxy</i>	<i>Morphology</i>	<i>Group</i>	<i>Galaxy</i>	<i>Morphology</i>	<i>Group</i>	<i>Notes</i>
NGC3379	E0	E,S0	MK487	Im	Irr	Odd (see text)
NGC4472	E1/S0	E,S0	NGC1569	Sm/Im	Irr	Reddened
NGC4648	E3	E,S0	NGC4670	SB pec	Irr	Peculiar
NGC4889	E4	E,S0	NGC3034	I0	Irr	Peculiar
NGC3245	S0	E,S0	NGC3077	I0	Irr	Peculiar
NGC3941	SB0/a	E,S0	NGC5195	I0 pec	Irr	Peculiar
NGC4262	SB0	E,S0	NGC6240	I0 pec	Irr	Peculiar
NGC5866	S0	E,S0	NGC3310	Sbc pec	Sb	Global Starburst
NGC1357	Sa	Sa	NGC3690	Sc pec	Scd	Global Starburst
NGC2775	Sa	Sa	NGC6052	Sm pec	Irr	Global Starburst
NGC3368	Sab	Sa	UGC6697	S pec	Irr	Global Starburst
NGC3623	Sa	Sa	NGC2798	Sa pec	Sa	Starburst Nucleus
NGC1832	SBb	Sb	NGC3471	Sa	Sa	Starburst Nucleus
NGC3147	Sb	Sb	NGC5996	SBd	Irr	Starburst Nucleus
NGC3627	Sb	Sb	NGC7714	S pec	Irr	Starburst Nucleus
NGC4750	Sbpec	Sb	MK35	pec	Irr	Peculiar
NGC2276	Sc	Scd	MK59	SBm/Im	Irr	HII Region
NGC4775	Sc	Scd	MK71	SBm	Irr	HII Region
NGC5248	Sbc	Sb	NGC3516	S0	E,S0	Seyfert I
NGC6217	SBbc	Sb	NGC5548	Sa	Sa	Seyfert I
NGC2903	Sc	Scd	NGC7469	Sa	Sa	Seyfert I
NGC4631	Sc	Scd	NGC3227	Sb	Sb	Seyfert II
NGC6181	Sc	Scd	NGC6764	SBb	Sb	Seyfert II
NGC6643	Sc	Scd	MK3	S0	E,S0	Seyfert II
NGC4449	Sm/Im	Irr	MK270	S0	E,S0	Seyfert II
NGC4485	Sm/Im	Irr	NGC1275	E pec	E,S0	Peculiar
			NGC3303	pec	Irr	Peculiar
			NGC3921	S0 pec	E,S0	Peculiar
			NGC4194	Sm pec	Irr	Peculiar

tion of the spectrum (Kennicutt 1992) indicates an erratic continuum.

In order to accurately test the methods for spectral reconstruction and classification it is first necessary to produce a set of galaxy spectra which resembles the spectra received from large redshift surveys. Details for the 2dF system (Taylor 1994) on the Anglo-Australian Telescope are used to degrade the Normal26 spectra, to simulate spectra from objects with a range of b_J magnitudes. Appendix A gives details about the spectral simulation procedure, detailing how the system response function, sky spectrum, fibre size and galaxy magnitude are incorporated into the simulations. It should be noted that it is difficult to predict the exact performance of the 2dF system and observations will obviously differ due to conditions, hence the simulations remain approximate, but demonstrate the level and variation of noise across the spectrum. We do not deal with the effect of aperture bias (the fact that a fibre can only sample a small area of a bright galaxy) in this paper, but acknowledge that it may cause discrepancies between the morphological and spectral type determined for a galaxy. Zaritsky et al. (1995) find that in general aperture bias would not constitute a large effect for the majority of galaxies, but they stress that it may still pose a problem in some cases. Figures 1-3 show examples of the simulated spectra for an elliptical galaxy, a spiral galaxy and an irregular emission line galaxy. In each case the original spectrum and simulations at a b_J magnitude of 19, 20 and 21 are shown. We refer to the original spec-

tra (from Kennicutt 1992) in the following sections as the ‘clean’ spectra, and we consider them not to contain noise. This is a reasonable assumption, since figures 1-3 show that the low S/N in the noisy simulations makes any noise in the original spectra negligible. Figures 1-3 indicate the importance of the emission lines for spectral classification at low S/N, and also reveal how the additional noise due to sky lines can produce false features such as those seen in figure 2, at $b_J = 20$ and $b_J = 21$.

For this method, the spectra must be compared in their rest frame, so we have used the redshifts (from Kennicutt 1992) for the galaxies to de-redshift the spectra (see Appendix A for the full procedure). The accuracy of the redshifts and resolution of the spectra determine the number of wavelength points which are used for the PCA.

A set of 900 spectra are produced in this way for each b_J magnitude. These 900 are based upon the Normal26 spectra, but each spectrum is simulated N_s times, where N_s is selected so that the final 900 spectra have the same morphological distribution as the ESO catalogue, as given in Table 1.

Since our initial data set is limited, this set of 900 spectra does not contain all the variation in a true observed set of spectra, such that we acknowledge that this analysis may lead to an optimistic rate of classification, but it demonstrates the methods we wish to use on more extensive sets of observed spectra.

The S/N per 8\AA resolution element averaged over all

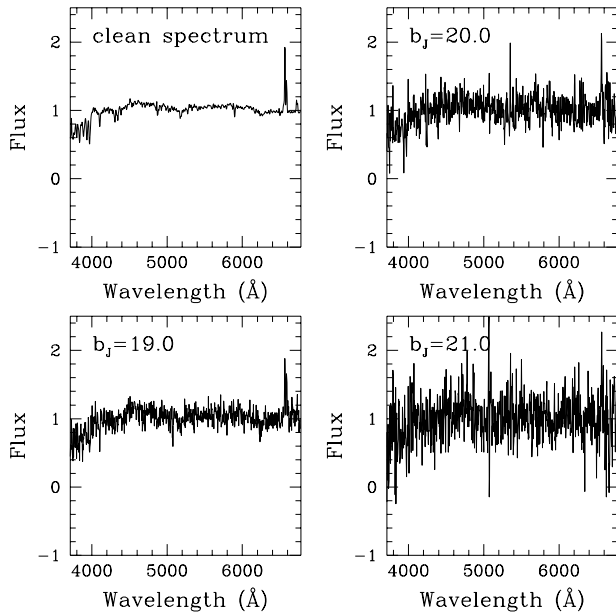


Figure 2. Simulated spectra based on NGC 3627 (Sb).

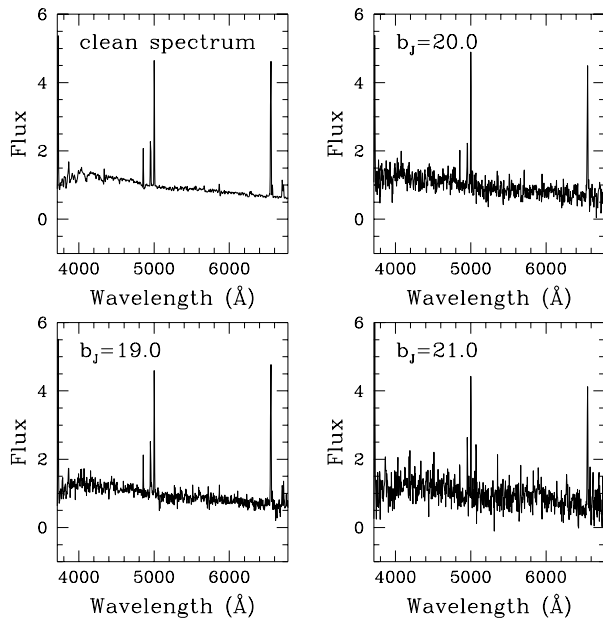


Figure 3. Simulated spectra based on NGC 4485 (Im).

wavelengths for all 900 spectra is calculated when a set of spectra is produced for a given b_J . Figure 4 shows a plot of this $\langle S/N \rangle$ against b_J computed in this way which can be used to associate the b_J magnitudes used in this paper with a general S/N spectrum from any source.

3 PRINCIPAL COMPONENT ANALYSIS

Principal Component Analysis (hereafter PCA) is a technique for both data compression and analysis (Murtagh &

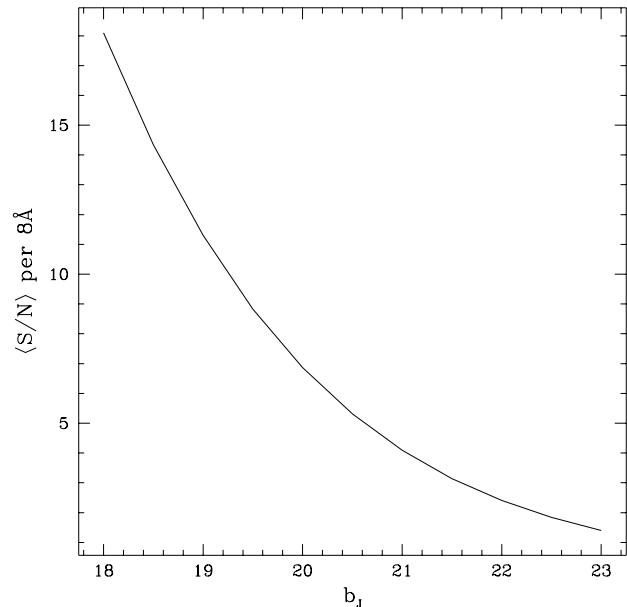


Figure 4. The variation in signal to noise per 8\AA resolution element measured for simulated spectra as a function of b_J .

Heck 1987) which can be employed to assess variations in galaxy spectra. By identifying the linear combination of input parameters with maximum variance, a set of new axes (principal components) is derived. A mathematical description is given in Appendix B. Computationally, we use the technique of Singular Value Decomposition to find the eigenvectors (or principal components) of the covariance matrix.

The question which arises is how to create the ideal set of principal components (or PCs) for galaxy spectra. The Normal26 spectra provide a useful data set, but they are not a representative sample of galaxy spectra in general. Ideally it would be best to define the PCs from the observed galaxy spectra of a large survey, but this data would be noisy and it is not clear at first how the noise would affect the PCA. Possibly filtering the spectra to reduce the noise level could improve the analysis, but this will lead to a loss of information.

As explained in section 2, a set of 900 clean spectra are created, based upon the Normal26 galaxies, which are sampled in 4\AA bins resulting in 768 wavelength bins for each spectrum. PCA is now conducted on the (768×768) covariance matrix using the techniques outlined in Appendix B. It should be noted that the speed of the PCA algorithm is dependent only on the number of wavelength bins used and not on the number of spectra (we chose 900 purely to produce a large morphologically weighted data set with many random variations).

3.1 Variance Scaling and normalization

In the analysis which follows, the spectra are all normalized to have the same total flux over the wavelength range considered, then the mean spectrum is subtracted from each of the input spectra. No further scaling is used.

We did examine the possibility of scaling each input flux

to unit-variance across the sample of spectra. This method is sometimes recommended for PCA analyses since it places each input on an equal footing. This would be advantageous when considering object attributes which are fundamentally different, for example if we were basing a classification system on galaxy colour, image ellipticity and OII equivalent width. For spectra, the problem is slightly different since all the inputs are fluxes for different wavelengths, hence the relative strengths of the inputs is important and should be retained in the analysis. Francis et al. (1992) investigate this problem for PCA on QSO spectra and choose not to scale by the variance.

Scaling by the variance means that the PCs for galaxy spectra at different noise levels are radically different, since at high S/N the PCA is sensitive to well correlated small features, but at low S/N these features are lost. Having chosen not to use this scaling we find the PCs only vary slightly with noise level, hence the PCs are intrinsic to the galaxy spectra themselves and not to particular observing conditions. In this case the PCs relate to both the magnitude and correlation of the features being chiefly concerned with regions of the spectra where the signal is strongest, such that they are not swamped by noise in the continuum. We also did the analysis with variance scaling, but found it gave a less reliable final classification, so we do not discuss this further.

Other possibilities are a normalization of each spectrum such that the integrated flux is the same, or alternatively such that the sums of the squares of the fluxes across the spectrum is unity (unit scalar product). This second case has certain mathematical benefits since it means that each spectrum can be represented by a unit vector in the parameter space. Connolly et al. (1995) consider these possibilities, but they find their results are not greatly affected by the choice of normalization. Hence for simplicity, we opt purely for a normalization to equal integrated flux.

The other operation we perform is to subtract the mean spectrum from each of the spectra in the set. This centres the points in the PC space about the origin, and makes the PCs easier to interpret.

3.2 The meaning of the principal components

Figure 5 shows the mean and the first 3 PCs for the data set based upon the Normal26 spectra and Figure 6 shows an enlargement of the first PC indicating the important features. These are computed without noise being added to the spectra, but when noise is added, the PC axes change very little. We quantify this affect in more detail in section 4. We find that the first PC accounts for 87% of the variance in the set of 900 clean spectra based on the Normal26 spectra. When the set is simulated at $b_J = 22$ ($S/N \sim 2.5$) the plot of the first PC is qualitatively the same, but only accounts for 11% of the variance, since the noise is producing large amounts of uncorrelated variance. Let us consider the meaning of the correlations which have been found in the Normal26 spectra. It can be seen that the first PC represents the correlation in the strength of the emission lines with the young stellar component. It shows that the OII (3727), OIII (4959 and 5007), $H\alpha$ (6563) and $H\beta$ (4861) lines are all linked with a blue continuum, demonstrating the effect of the ionizing photons from young stars exciting the interstellar medium

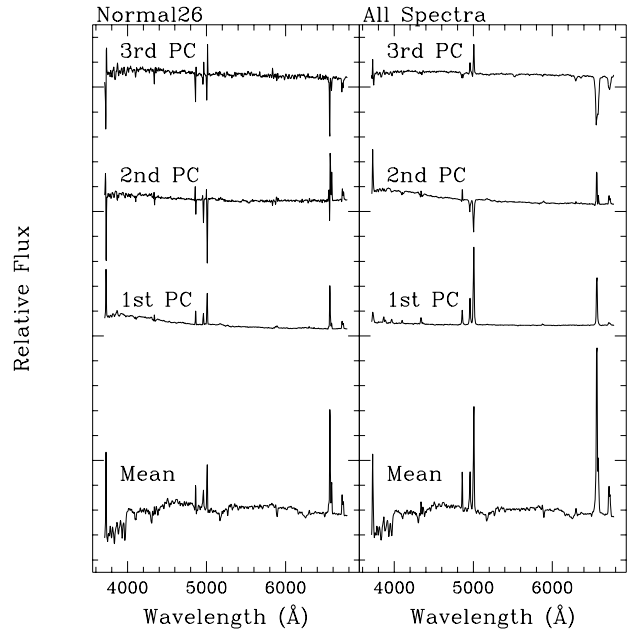


Figure 5. Principal components for the Normal26 spectra and for the entire set, without additional noise.

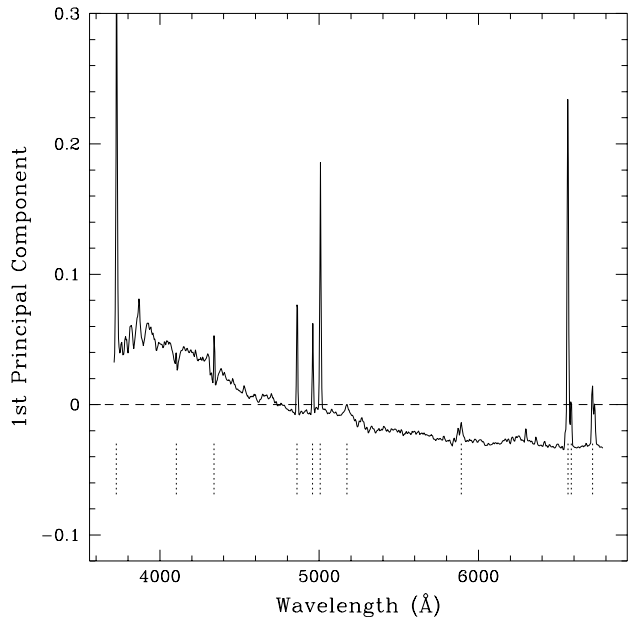


Figure 6. The first principal component for the Normal26 spectra, indicating some of the important features.

resulting in strong emission lines. The second PC allows for a range of ionization levels of the galaxies, since the oxygen and hydrogen lines are anti-correlated. The third PC indicates numerous other correlations between absorption and emission features. A parallel study involving PCA with the Kennicutt sample of galaxies (Sodré & Cuevas 1996) finds similar principal components.

It is hoped that the amplitude of a small number of these eigenspectra in any particular spectrum will be suffi-

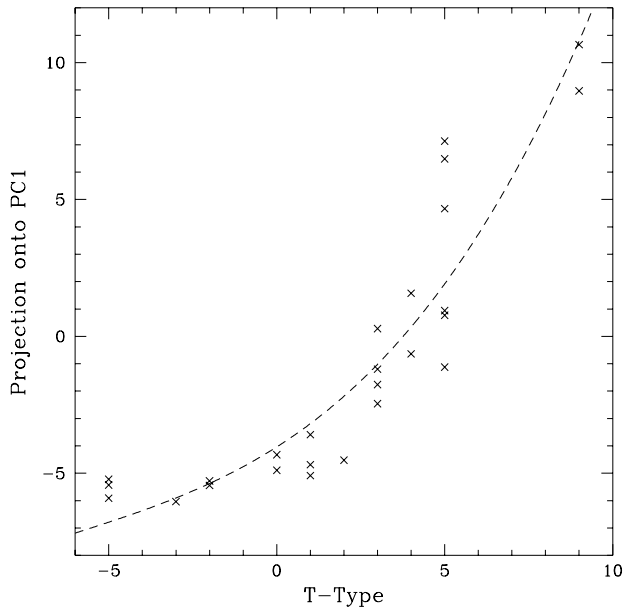


Figure 7. The projection onto the first principal component plotted against T-Type for the Normal26 spectra.

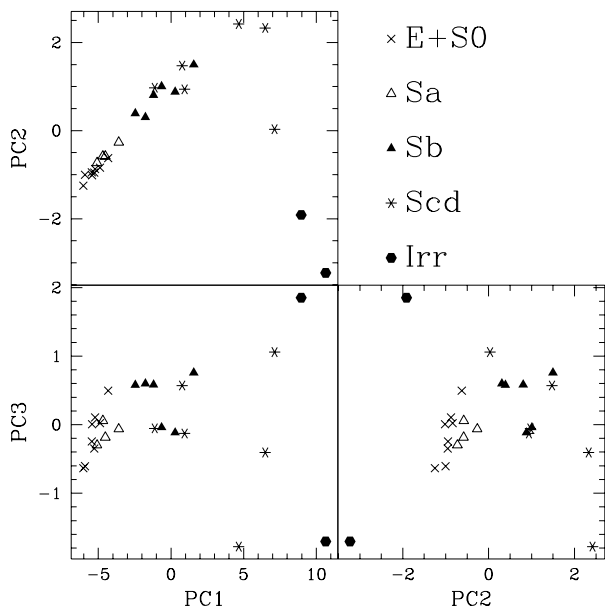


Figure 8. Projections onto the first 3PCs plotted against one another for the Normal26 spectra.

cient to spectrally classify the galaxies. Since the projections onto the eigenspectra use information from the entire spectrum this provides a much less noisy measure than comparing the strength of particular features. A simple indication that this may be true can be seen in Figure 7, which indicates a correlation between the projection (see Appendix B) of each of the Normal26 spectra onto the first PC and the morphological type of the galaxy on the T-Type system (de Vaucouleurs 1959; de Vaucouleurs 1963). A simple fit to

this relation (as shown by the dotted line) allows the projection onto the first PC to be used to classify the galaxies into a specific T-Type. This has been used later to provide a comparison to the classifications using the ANN. Further evidence of an underlying spectral sequence can be seen in Figure 8 where the projections onto the first three PCs are plotted against each other, with the symbols representing different morphological types. Segregation in this plot indicates that the PCs are capable of differentiating between galaxy morphologies and that the Hubble sequence is clearly evident in the Normal26 spectra and not just their visual appearance on the sky. The Hubble sequence appears as a combination of PC1 and PC2, indicating that although one spectral parameter is sufficient to explain the sequence up to Sc galaxies, a second parameter (allowing for variation in ionization) becomes very important for late type and irregular galaxies, where strong star formation leads to high ionization levels. In their study, Sodr e & Cuevas (1996) found that stellar synthesis models (Bruzual & Charlot 1995) with different ages and star formation rates form a similar sequence when projected onto PCs derived from the Kennicutt (1992) sample of galaxies.

Figure 5 also shows the mean and first three PCs for the entire data set, including the Normal26 and the Unusual29 spectra. These are derived by the same method as described above. The morphological mix from Table 1 is again used, but note that this does not necessarily represent a true spectral mix. This means that the galaxies with unusual features are over represented, but this allows their affect on the PCA to be seen. In this case, the first PC is entirely due to the emission line strength, since the PCA is dominated by the emission line objects. The young stellar continuum is evident in the second PC along with anti-correlations between the major emission lines. In this respect the first PC from the Normal26 spectra is evident as a combination of the first and second PCs of the entire data set. The third PC is now quite different, and displays the broad hydrogen lines characteristic of the galaxies with Seyfert nuclei.

4 RECONSTRUCTIONS FROM NOISY SPECTRA

We now proceed to investigate the effect of noise on the PCA technique. It would be useful to perform PCA on a large set of observed spectra, such as the 2dF spectra, since this set would contain all the possible variation in galaxy spectra and is representative of the local universe. However these observed spectra would be noisy and this may affect the location of the principal components. Using the spectral simulations we can assess the nature of this effect, by measuring the ability of the PCs to reconstruct the original spectrum. Appendix B explains how a reconstruction of the original data can be found using only a small number of PCs. Taking a set of noisy simulated spectra we can reconstruct them and define the total Residue R for the set as

$$R = \frac{1}{NM} \sum_{ij} (S_{ij}^r - S_{ij})^2, \quad (1)$$

where the sum is over all N spectra and M wavelengths, S_{ij}^r is the flux of the i th reconstructed spectrum at wavelength j ,

and S_{ij} is the flux of the original clean i th spectrum at wavelength j . This reconstruction technique suggests the useful ability of PCA to disregard the noise, which is assumed to be uncorrelated. The major correlations in the signal are selected by the PCA, and the noise only interferes with the later PCs, such that a reconstruction using the most significant PCs can eliminate much of this uncorrelated noise. To demonstrate this effect, figure 9 shows a plot of R against the number of PCs used in the reconstruction. Seven different cases are considered and these are listed in Table 3. In each case two sets of spectra are used. One set is used to define the principal components and is labeled ‘Spectra_{PCA}’. The other set is reconstructed to find the Residue R and is labeled ‘Spectra_{REC}’. This reflects the possibility of defining the principal components prior to the observations using a smaller set of high quality spectra. However this would probably entail using a limited data set, so Table 3 also contains a case where only half of the Normal26 spectra have been used to define the PCs. Each set contains 900 spectra mimicking the morphological mix given in Table 1. There is one other possibility considered in Table 3, that of filtering the spectra prior to the reconstruction and we have used the technique of Wiener filtering to demonstrate this effect (see section 4.2).

4.1 Reconstruction results

Referring to Figure 9, we can see that the smallest R value is obtained using the noise free spectra for the Spectra_{PCA} and the Spectra_{REC} sets (line a). This is to be expected and represents the ideal condition, but one which is not available for a real observation since the underlying signal is not known. A set of clean spectra, such as the spectra we are using, could be used to form the PCs for use with observed noisy spectra, as lines b and e demonstrate. However the line d indicates that when only half of the spectra are used in the PCA the result is considerably worse, which suggests that a small set of spectra should not be considered representative of a larger ensemble. Therefore it would be better to derive the PCs from the noisy spectra themselves. This condition is shown by lines c and g for two different noise levels. It can be seen that for $b_J=19$ (line c) about 8 PCs still contain meaningful information, but the later PCs are merely reconstructing the noise (as indicated by a rise in R). This means that the optimal reconstruction is found by limiting the PCs used to the point at which R is found to be a minimum and this then represents the entire meaningful information that can be extracted from the spectrum. Line g indicates that for very noisy data only the first PC is still meaningful.

So given a set of noisy spectra, it is reasonable to perform PCA on the spectra themselves, but to acknowledge the fact that only a certain number of the PCs are useful, with this number depending on the S/N of the spectra. If a set of high S/N spectra are available, using the PCs from these may extract more of the information (see lines e and g), but in this case the assumption that the noisy spectra can be well described by the PCs from the clean spectra must be made, and (as line d shows) this is not always true. Figure 10 indicates how the optimal number of PCs (i.e. the number which gives a minimum in R) varies with b_J when Spectra_{PCA} and Spectra_{REC} are both simulated at

Table 3. The seven PCA combinations used for analysis of reconstruction errors, with the notation for Figure 9.

Spectra _{PCA}	Spectra _{REC}	Notation in Figure 9
Clean	Clean	a
Clean	$b_J = 19$	b
$b_J = 19$	$b_J = 19$	c
Clean, half data set	Clean	d
Clean	$b_J = 22$	e
$b_J = 22$	$b_J = 22$ filtered	f
$b_J = 22$	$b_J = 22$	g

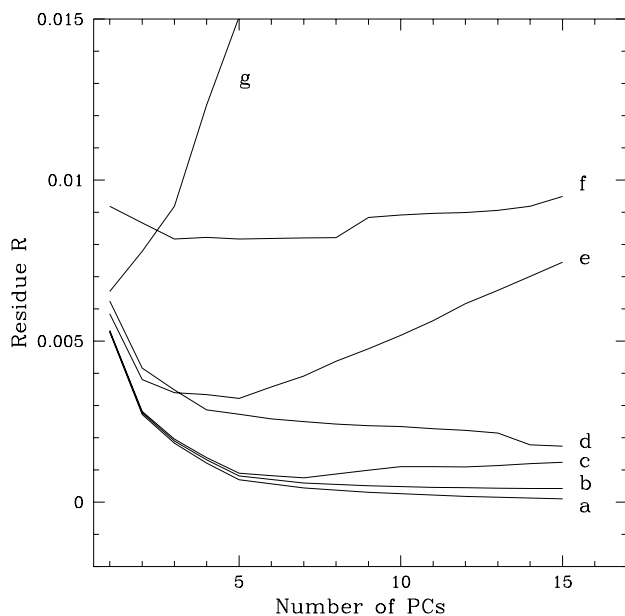


Figure 9. Reconstruction errors for different sets of spectra. See Table 3 for explanation of line labels.

b_J . The exact normalization of this graph depends on the specific data set being considered, including factors such as the number of spectra, and the wavelength sampling. For a very large set of data from a big redshift survey it may be expected that more PCs would be significant.

4.2 Wiener Filtering

An alternative method for extracting the meaningful information from the spectra is Wiener filtering in Fourier space (see Press et al. 1992 for a full description). This involves a smooth truncation of modes in a data independent basis, as opposed to the PCA which involves a sharp truncation in a basis which is adapted to the data. In Fourier space, let $S(k)$ be the true spectrum of a galaxy, then the observed spectrum $O(k)$ is given by

$$O(k) = S(k) + N(k), \quad (2)$$

where $N(k)$ is the Fourier transform of $n(\lambda)$ (the noise at each wavelength). Let us define a linear filter in Fourier space, $W(k)$ by

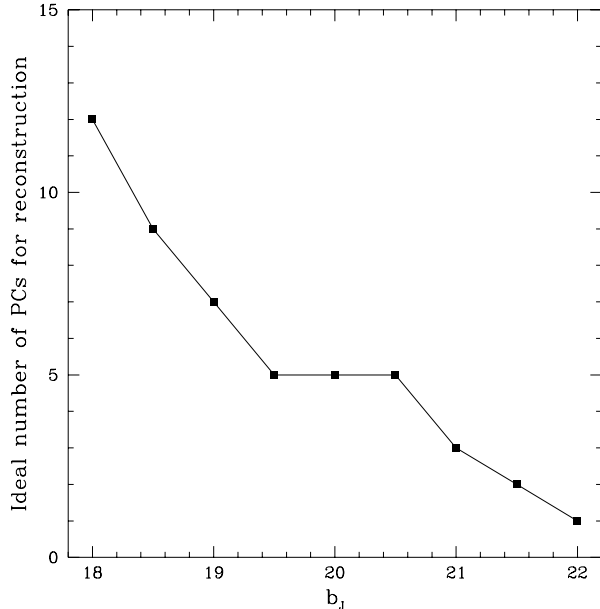


Figure 10. The optimal number of PCs for spectral reconstruction as a function of b_j .

$$S_r(k) = O(k)W(k), \quad (3)$$

where $S_r(k)$ is the best reconstruction of $S(k)$. By a least squares minimization with respect to $W(k)$ we find

$$W(k) = \frac{|S(k)|^2}{|S(k)|^2 + |N(k)|^2}, \quad (4)$$

where we have ignored terms involving $S(k)N(k)$ since the noise and signal are considered to be uncorrelated. From equation (4), we define $W(k)$ as the Wiener filter.

For this method we must first assume an underlying signal $S(k)$ in the spectrum. To do this we have formed 5 templates, one for each of the groups given in Table 1 by taking the mean of the Normal26 spectra in that class. We then take each noisy spectrum and compare it to the 5 templates and look for the best template in the least squares sense. This template is then used as the prior for the Wiener filtering. In addition this template matching method is a simple method of classification where a galaxy spectrum can be allocated to the group whose template it matches best. We use this later as a comparison to the classifications from the ANN.

Wiener filtering can be seen as an alternative technique to produce a reconstruction from a noisy spectrum and it is interesting to compare the PCA reconstructions and the Wiener reconstructions. This comparison can be seen in Figure 11 for different levels of noise. It can be seen that the Wiener filtering reduces the noise, but also smooths the signal, such that at low S/N the features are lost and only the rough continuum shape remains. In comparison the PCA reconstructions retain much more of the information in the spectrum, producing a reasonable reconstruction of the spectrum to a b_j of 22. At low S/N the noise causes some spurious

effects, but many of the distinguishing spectral features, in this case $H\alpha$ and the 4000Å break are retained. In order to make this reconstruction, the noisy spectrum is assumed to be characteristic of the set of spectra used to produce the principal components. This means that the reconstruction conforms to the correlations laid by the PCA. For some data sets it is possible that PCA would not provide a good description of the data and Wiener filtering in Fourier space would be the preferred method. Ideally a very large set of spectra is required for the PCA, such that the complete range of spectral possibilities is encompassed, and we hope to apply the techniques given here to such data sets in the future. Referring back to figure 9, line f is the result of first Wiener filtering the spectra before projecting onto the PCs. This removes much of the noise so that the line does not rise so rapidly, but the action of the filtering also removes much of the meaningful signal in the spectrum so that the reconstruction is never as good as the single PC reconstruction based on the noisy data (line g).

4.3 Combining Wiener filtering and PCA

As an aside, we can see in the previous section that the PCA, which takes into account correlations between the features, produces a far superior reconstruction than the Wiener filter used in Fourier space, but we have also noted that PCA reconstructions of noisy data should be restricted to only the first few PCs, since the noise interferes with the later PCs. The PCA works better than the Fourier representation because the PCA axes are chosen specifically to represent the data, whereas the Fourier axes are a generalized orthogonal set and not specific to the data being considered. The Wiener filter is used to produce a smooth cutoff of the Fourier modes so that the noisy modes are reduced in weight. Such a procedure could also be used with the PCA where, instead of truncating after a determined number of PCs, a filter is used which merely reduces the weight of the later PCs. In this paper, we actually need a direct truncation of the PCs, since we want to minimize the number of inputs to the ANN (hence reducing the number of free parameters of the network), but for a general spectral reconstruction the filtered PCA is a promising idea.

5 SPECTRAL CLASSIFICATION WITH AN ARTIFICIAL NEURAL NETWORK

Figures 7 and 8 show that the visual morphology and the spectrum of a galaxy are related and that this relation is embodied in the projection onto the PCs. This suggests that a useful method for the classification of galaxy spectra is to associate each spectrum with a morphological type. This would allow the morphology of galaxies to be examined at far greater distances and with less subjectivity than conventional examination of galaxy images. We have trained an ANN to assign morphological classifications to galaxies, based on their spectra as represented by the projections onto a small number of PCs.

For each spectrum, the ANN produces an output classification which is a non linear function of the inputs. The form of the function is parameterized by a set of weights which are adjusted so that the output matches the known

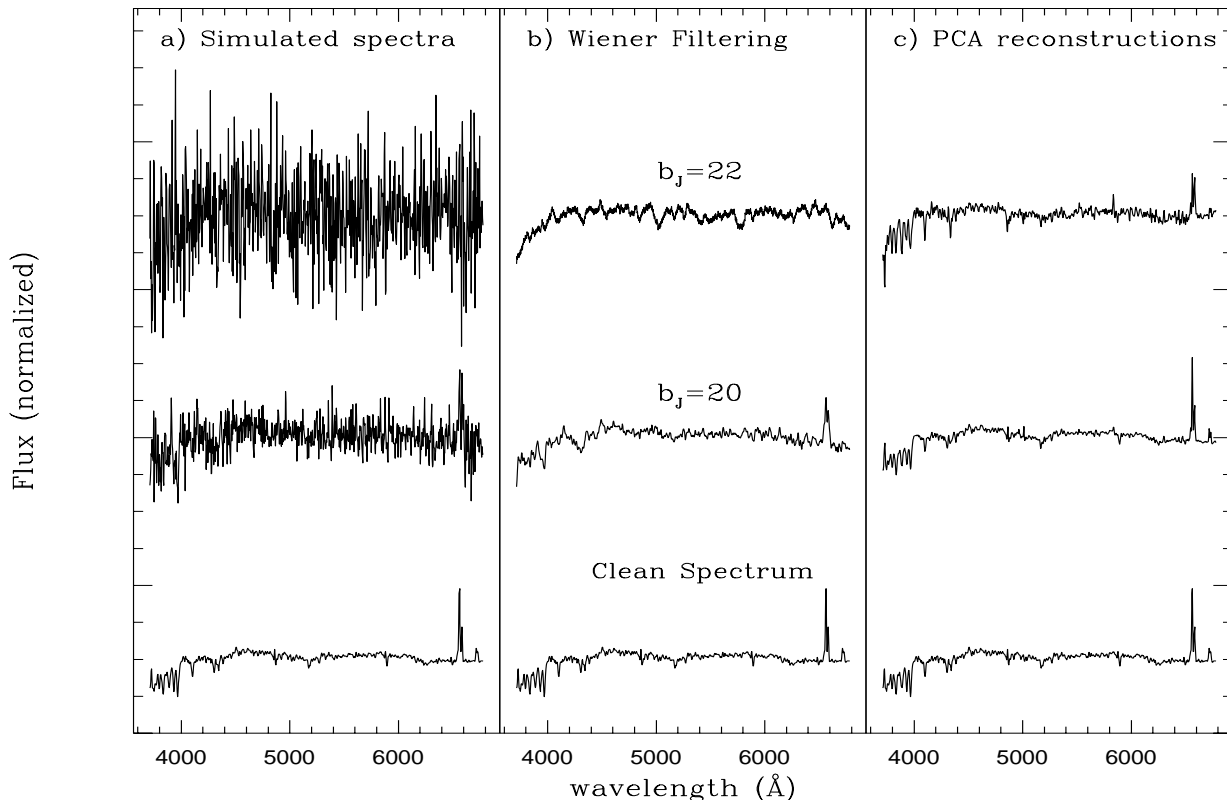


Figure 11. Comparison of spectral reconstructions for NGC3627 (Sb). a) The simulations for $b_j=20$ and $b_j=22$. b) Wiener filtering of the noisy spectra using a group template (see text). c) PCA reconstructions of the noisy spectra based upon 8PCs derived from the Normal26 spectra.

classifications for a training set. To be precise, the effect of training the ANN is to perform a minimization across the ANN weights vector (\mathbf{w}) given a set of inputs \mathbf{x}_i for the i th galaxy (e.g. the spectrum as represented by the PCs) and known outputs T_i (e.g. the morphological group). This is done by minimizing the cost function

$$E = \frac{1}{2} \sum_i [T_i - F(\mathbf{w}, \mathbf{x}_i)]^2, \quad (5)$$

where the non-linear function $F(\mathbf{w}, \mathbf{x})$ represents the network and the summation is over the training set of spectra.

Once the weights are set, the training is complete and the ANN can be used to classify the complete galaxy sample. A full description of the ANN as a tool for data analysis is given in Appendix C (for further detail see Lahav et al. 1996). We used a quasi-newton ANN code with the network architecture designed to allow the projections onto the first 8 PCs (derived from a set of spectra simulated at $b_j = 19.0$) to be used as input to the net and a single output being the morphological group. Between the input and output layers we chose a single hidden layer with 5 nodes, which provides a level of non-linearity in the classification. We experimented with different numbers of nodes and hidden layers and decided upon the 8:5:1 setup as the simplest architecture which gave consistently successful results. Simpler architectures were not reliable and more complex nets

failed to improve the results. The output from the ANN could then be scaled and binned to give the five classes as defined in Table 1. The training process involved weight decay, which acts as a regularisation during the training, preventing erratic variations in the weights. The quasi-newton minimization and the use of weight decay are discussed in more detail in Appendix C.

We chose to use 8 PCs based upon the results in section 4, which indicate this to be a reasonable compression of the data for the S/N levels we considered. We produced a set of 900 simulated spectra at each of 9 values of b_j between 18 and 22, resulting in a total set of 8100 spectra. One third of this set was then repeatedly submitted to the ANN as a training set until the error between the ANN classification and the known morphological types of the galaxies began to converge. The ‘trained’ net was then used to classify the complete set of 8100 spectra onto a continuous scale defined by the group G number as given in Table 1. In this way the scaled output from the ANN was a single number in the range 0.5 to 5.5 and an output group was found by allocating the galaxy to the nearest group bin. These classifications could be compared with the known types of the galaxies to give a level of success at each magnitude. The ANN is trained, and spectra classified, ten times using this method to give a mean and standard deviation for the percentage of galaxies allocated to the correct group, and these results can be seen in Figure 12. In addition, if only a 3 group

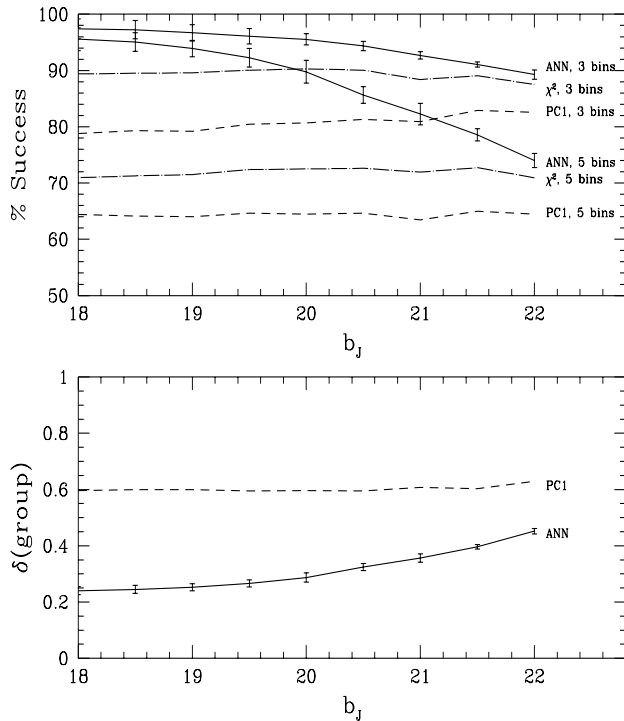


Figure 12. The percentage of ANN classifications which agree with the known morphological types for 5 and 3 classes, based upon the Normal26 spectra. Also shown is the success of χ^2 template matching and classification based solely on PC1. The lower graph indicates the variation in $\delta(\text{group})$ against b_j for classifications from the ANN, and PC1 alone.

classification is required, the Sa, Sb and Scd groups can be combined to give one large group of spirals. The success rate for this 3 group binning is also shown in figure 12.

A further measure of success is the $\delta(\text{group})$ statistic given by

$$\delta(\text{group}) = \sqrt{\frac{1}{N} \sum_i (G_i - A_i)^2}, \quad (6)$$

where the sum is over the N spectra (in this case a set of 900), G_i is the actual group to which the galaxy belongs, as defined in table 1 and A_i is the neural net classification on a continuous scale from 0.5 to 5.5.

These results are encouraging, showing that the morphological variation in the Normal26 galaxies is well represented in their spectra and that the PCA/ANN technique is capable of extracting this information even with very noisy spectra.

Figure 12 indicates several other lines for comparison. Two of the lines refer to the classification success when a classification based solely upon PC1 is used. A simple relation between T-Type and PC1 is assumed (as indicated by the line on Figure 7) and the results shown using 5 and 3 groups. $\delta(\text{group})$ was also calculated for this method so that it can be compared with the ANN. The classification based solely on PC1 is found not to be ideal, although it is stable to high noise levels (since PC1 is the most meaningful cor-

relation in the data and should not be greatly affected by noise). It is clear that the ANN is capable of better classifications using more of the principal components than the single PC result. The later components are affected by noise to a greater extent, so the ANN classification does fall as the noise level increases.

The other two lines on Figure 12 refer to a classification based on χ^2 template matching, from the procedure in section 4.2. This indicates a reasonable level of success, but is unable to capitalize on the extra information at high S/N which allows the ANN to refine the classifications. Since the template matching gives a discrete group output, $\delta(\text{group})$ is not calculated for this method.

6 AGREEMENT OF MORPHOLOGICAL AND SPECTRAL TYPES

We now have an ANN which has been trained to relate the spectral type and morphological type of normal galaxies, using the projections onto the first eight PCs (derived from the Normal26 morphologically weighted sample). We use this to classify the Normal26 and the Unusual29 spectra without noise, to gain an indication of the agreement between spectral and morphological type. The results can be seen in figure 13. The Normal26 spectra form a reasonable sequence, with a degree of scatter in each group. This scatter is related to the $\delta(\text{group})$ statistic plotted in Figure 12 (but note that $\delta(\text{group})$ is summed over a complete morphological sample of 900 spectra at a particular noise level). Some overlap between the groups can be seen, verifying the fact that we are dealing with a sequence in galaxy type and not discrete classes. The agreement between morphological and spectral type indicated in Figure 13 substantiates the conclusions of the PCA analysis (Figures 7 and 8) which suggested strong links between spectra and morphology. It is reassuring to see that the traditional Hubble classification system is telling us about stellar and gas content in addition to the morphology of the galaxy.

As expected, the Unusual29 spectra do not conform to this morphology-spectrum relation. In general, the unusual spectra which have been morphological classified into groups 1 to 4, produce a higher spectral class from the ANN. This is due to the presence of starbursts, Seyfert nuclei and emission features which increase the ‘activity’ in these spectra, above that of a normal galaxy for that class. The unusual spectra in morphological group 5 contain galaxies with T-Types greater than 8.5, which include irregular and peculiar types along with extreme emission galaxies. The irregular emission line objects are classified correctly as being extreme in spectral class (group 5), but the peculiar galaxies reveal a range of spectral features, such that they are classified into a variety of spectral classes. We can investigate some particular cases which have been highlighted in Figure 13, and look at the spectra and comments given in Kennicutt (1992). The morphologically peculiar galaxy NGC 3077 has been spectrally classified by the ANN as a late Sb galaxy (ANN output group 3.15) which broadly agrees with the comments given in Kennicutt (1992) that this spectrum is similar to that of a normal Sc. In contrast, the spectrum of NGC 5195 has been spectrally classified as an elliptical by the ANN (ANN output group 1.25), whereas Kennicutt (1992) comments that it

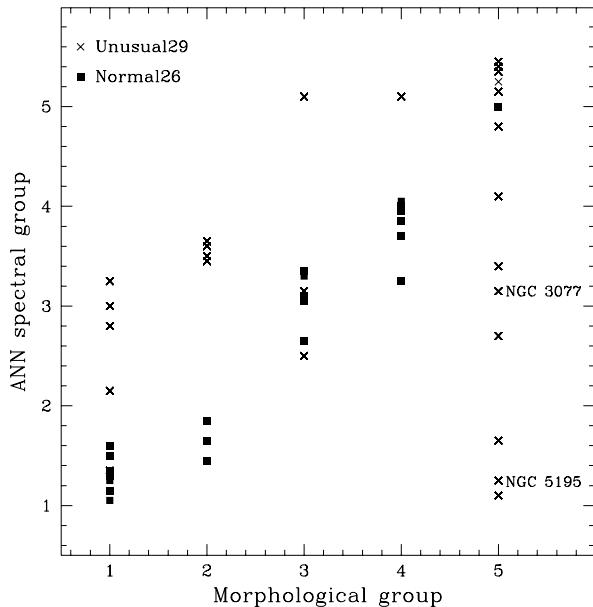


Figure 13. The Agreement of spectral and morphological classifications for the Normal26 spectra and the Unusual29 spectra.

resembles an old stellar population with weak emission lines, or an ‘E+A’ galaxy. From a sample of this size, we cannot say that the ANN is telling us anything very new, but it can be seen that the ANN is producing a consistent spectral classification which broadly agrees with a visual analysis of the spectra. It can clearly be seen in Figure 13 that the Unusual29 galaxies show very little agreement between morphological and spectral type, so in an observed sample, it would be useful to separate the normal from the unusual spectra. As Figure 7 shows, the Hubble sequence is clearly evident in relations between the PCs, so it is reasonable to assume that the unusual spectra do not have this uniformity, for example they may show discrepant emission and absorption features, or indicate strong ionization from a Seyfert nuclei without the presence of a young stellar population. To test this hypothesis, we have taken the Normal26 and Unusual29 spectra, simulated them at different noise levels, but without any morphological weighting, and run the PCA routine on the entire set. We then train the neural net (using 8 PCs) to output 0 if a galaxy is one of the Normal26, or a 1 if the spectrum is a member of the Unusual29. When the ANN is trained, we ask it to reclassify the galaxies itself into these two bins. We find that at $b_J = 19.7$ about 95% of the spectra have been classified correctly in this way.

7 DISCUSSION

We demonstrate in this paper that the combination of the PCA technique and the ANN analysis produces a useful classification tool. The PCA is useful in three ways in our technique: (i) It allows a transformation of the data to a more useful set of axes, to reveal segregation in the sample. (ii) It allows a reconstruction of a low S/N spectrum. (iii) It provides an economic set of input parameters for the ANN. We have shown that a limited number of PCs convey

the underlying information in the spectra, and beyond a certain number of PCs (defined by the noise level) the PCs are not producing useful information. When the data is restricted to the Normal26 galaxies, the projections onto the first few PCs reveal segregation in the data which is chiefly due to the morphological variation in the spectra. If the Unusual29 spectra are included, the variance in the data is due to parameters other than purely the morphological type. We show that the PCA is best executed on the observed spectra themselves, even if they are noisy, since the PCs are then highly relevant to that data set. The alternative approach of projecting the noisy data onto PCs derived from a small set of high quality spectra can be used, but in this case, the PCs do not necessarily describe the entire range in the larger set of observed spectra.

The results from the ANN suggest that a good agreement between spectral and morphological type can be attained for the Normal26 spectra and that a better classification can be made using this approach than a simple χ^2 fit to a set of templates. We have also shown that classification information is not restricted to the first principal component, such that a classification based purely on this is not very successful. As expected, little agreement is seen between the morphology and spectra of the Unusual29 galaxies. One way to proceed would be to separate these spectra from the main sample, and then to analyse only the normal galaxies with reference to the Hubble sequence. We show that it is also possible to use an ANN to make such a distinction. This would leave a set of unusual spectra which could be classified separately, or analysed using an alternative method, such as cluster analysis in the PC space, or one of a variety of unsupervised data analysis methods which look for trends or groupings in the data. The ability to highlight unusual spectra would also prove useful in detecting spectra with bad sky subtraction, inaccurate fluxing, or incorrect redshift determinations, so that these could be dealt with separately. The small data set used in this analysis means we are unable to draw rigorous conclusions as to the full variation of galaxy spectra. We hope to remedy this situation in the near future with similar analyses of larger observed data sets from existing redshift surveys and spectroscopic environmental studies.

We intend to use the the results of this paper as the basis for classifying the spectra from the 2dF Galaxy Redshift Survey. We have shown that a five class classification is obtainable to the proposed magnitude limit of the survey ($b_J = 19.7$), but this paper also demonstrates that it is not necessarily advantageous to restrict the classification to discovering the morphological types of the galaxies. It may be better to extend the classification into classes based entirely on the spectral type. The PCA alone can reveal such subsets in the data and will provide a powerful tool when used on a large data set. For the ANN to operate well, a number of the spectra need to be used as a training set. Several options are available, such as using morphological classifications from those images bright enough to be classified by eye, a manual analysis of the high quality spectra or the use of population synthesis models. A recent investigation (Sodr e & Cuevas 1996) has successfully related the positions of observed spectra and model spectra on the PC1/PC2 plane and this suggests that an ANN trained with model spectra

may be able to provide interesting insights into the physical factors determining galaxy spectra.

8 CONCLUSION

We have demonstrated a method for the classification of low S/N spectra using simulations based upon the set of galaxy spectra presented in Kennicutt (1992). We have developed the simulations to resemble spectra from the 2dF Galaxy Redshift Survey and show that reliable classifications, with more than 90% of the normal galaxies correctly classified, can be expected to the magnitude limit of the survey ($b_J = 19.7$). This may be optimistic, since our small data set does not encompass the full variation in galaxy spectra, but our results strongly suggest that the methods in this paper will provide an interesting analysis technique when the 2dF Galaxy Survey spectra are available. We have explored the effect of noise on the Principal Component Analysis of spectra and demonstrate that an ANN is a useful tool for the classification of noisy spectral data. We show that the ANN classification is more successful than either a χ^2 template matching approach or a classification based solely on the projection onto the first principal component. We have also investigated the agreement of spectral and morphological type and discussed a method to separate normal from unusual galaxy spectra.

ACKNOWLEDGMENTS

The authors would like to thank C. Bailer-Jones, R.S. Ellis, P.J. Francis, J.S. Heyl, M.J. Irwin, A. Naim, L. Sodr e, Jr., M.C. Storrie-Lombardi, T. von Hippel, and the 2dF Galaxy Survey collaborators for useful discussions concerning spectral classification. We would also like to thank B. Ripley for making the ANN code available.

REFERENCES

Bruzual G., Charlot, S., 1995, Galaxy Isochrone Synthesis Spectral Evolution Library (GISSEL95)
 Connolly A.J., Szalay A.S., Bershadsky M.A., Kinney A.L., Calzetti D., 1995, AJ, 110, 1071
 de Vaucouleurs G., 1959, in : Fl ugge, S. (ed.) : Handbuch der Physik 53, 275, Berlin : Springer-Verlag
 de Vaucouleurs G., 1963, ApJS, 8, 31
 Francis P.J., Hewett P.C., Foltz C.B., Chaffee F.H., 1992, ApJ, 398, 476
 Hertz J., Krogh A., Palmer R.G., 1991, Introduction to the Theory of Neural Computation. Addison-Wesley, Redwood city, California
 Hubble E., 1936, The Realm of Nebulae, Yale University Press, New Haven
 Humason M.L., 1936, ApJ, 83, 18
 Kennicutt R.C., 1992, ApJS, 79, 255
 Lahav O. et al., 1995, Science 267, 859
 Lahav O., Naim A., Sodr e L., Jr, Storrie-Lombardi M.C., 1996, MNRAS, submitted
 Lauberts A., Valentijn E.A., 1989, The Surface Photometry Catalogue of the ESO-Uppsala Galaxies, ESO
 MacKay D.J.C., 1992, PhD thesis, Caltech
 Maddox S.J., Efstathiou G., Sutherland W.J., Loveday J., 1990, MNRAS, 243, 692

Morgan W.W., Mayal N.U., 1957, PASP, 69, 291
 Murtagh F., Heck A., 1987, Multivariate Data Analysis, Reidel, Dordrecht
 Naim A., Lahav O., Sodr e L., Jr, Storrie-Lombardi M.C., 1995, MNRAS, 275, 567
 Press W.H., Teukolsky S.A., Vetterling W.T., Flannery B.P., 1992, Numerical Recipes, 2nd edition, Cambridge University Press, Cambridge.
 Ripley B.D., 1993, Statistics and Images, ed. K.V. Mardia, Abingdon, Carfax
 Rumelhart D.E., Hinton G.E., Williams R.J., 1986, Nature, 323 533
 Smyth R.J., 1982, Observatory, 102, 225
 Sodr e L. Jr., Cuevas H., 1994, Vistas in Astronomy, 38, 287
 Sodr e L. Jr., Cuevas H., 1996, MNRAS, submitted
 Storrie-Lombardi M.C., Lahav O., Sodr e L. Jr., Storrie-Lombardi L.J., 1992, MNRAS, 259, 8p
 Storrie-Lombardi M.C., Irwin M.J., von Hippel T., Storrie-Lombardi L.J., 1994, Vistas in Astronomy, 38, 331
 Taylor K. 1994, in Maddox S.J., Aragon-Salamanca A., eds, Proc. of the 35th Herstmonceux Conference, Wide field spectroscopy and the distant universe. World Scientific publishing, p.15
 von Hippel T., Storrie-Lombardi L.J., Storrie-Lombardi M.C., Irwin M., 1994, MNRAS, 269, 97
 Zaritsky D., Zabludoff A.I., Willick J.A., 1995, AJ, 110, 1602

APPENDIX A: SIMULATIONS OF GALAXY SPECTRA

In order to assess the performance of our classification and reconstruction procedures in the presence of noise, we have simulated spectra as they would appear with an 1800 second integration using the 2dF system (Taylor 1994) on the Anglo-Australian telescope. This system consists of a prime focus corrector giving a field of view 2 degrees in diameter, within which 400 optical fibres can be accurately placed at the positions of galaxies. Each fibre covers a 2" diameter region of sky and feeds the light to a highly efficient spectrograph. Using a 300B grating will give a resolution of 8  and the present CCD detectors sample the spectra at 4  per pixel. We plan to survey a large number of galaxies brighter than $b_J = 19.7$ using this instrumental set-up, and the simulations are specifically designed to reproduce the data expected for our survey. However, since the simulations include all the normal observational effects, they also provide a reasonable approximation to data for other redshift surveys.

As our starting point we take a sample of high signal-to-noise spectra (Kennicutt 1992) and redshift each galaxy spectrum to $z=0.1$, which is the expected median redshift for our planned survey. Then we re-sampled the spectra using 4  pixels. The $b_J - V$ colour is calculated from each spectrum so that the V magnitude corresponding to any particular b_J can be estimated. We scale each spectrum to the relevant V magnitude by first normalising it so that the mean flux between 5550  and 5600  is unity. Then, by considering the flux from a $V = 0$ object, the 95100 cm^2 collecting area of the AAT and an exposure time of 1800 seconds, we calculate the number of galaxy photons at each wavelength. Ideally the normalization would be done at 5500  (being the characteristic wavelength of the V filter) but at $z=0.1$ the OIII lines obscure this area of the continuum and since

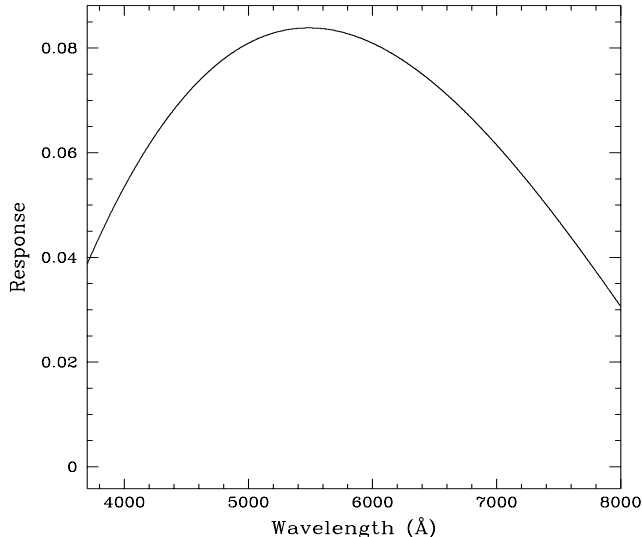


Figure A1. The response function used for the spectral simulations, assuming the 300B grating.

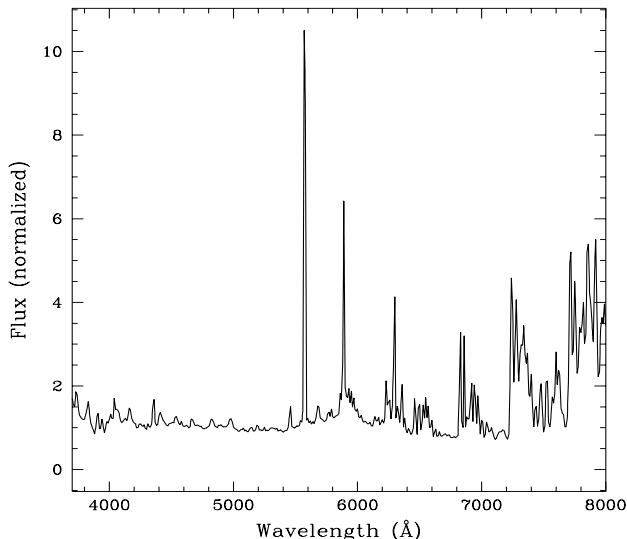


Figure A2. The sky spectrum used for the spectral simulations.

the continuum is relatively flat over this short region the difference is minimal.

The throughput of the 2dF system has been predicted for a variety of configurations using detailed modeling of the instrumental optics (Taylor 1994). The overall system efficiency predicted for observations of a point source with zero seeing observed with the 300B grating is shown as a function of wavelength in Figure A1, and we multiply each spectrum by this response function.

For galaxies larger than the 2" diameter fibres, only a fraction of the total light enters the fibre, and this fraction, F , depends on the surface brightness profile of the galaxy. We have estimated the mean value of F as a function of magnitude using the observed surface brightness profiles of galaxies in the APM galaxy survey (Maddox et al. 1990).

For each galaxy we numerically integrate the profile out to a radius of 1", and compare this to the total magnitude of the galaxy. At $b_J=19.7$ we find that an average galaxy contains 0.18 ± 0.01 of its total light within a radius of 1" from the galaxy centre. Using galaxies with $21 < b_J < 19$ and measuring F in 0.2 magnitude bins we find an approximate relation

$$F = kL^{-0.4}, \quad (\text{A1})$$

where L is the galaxy luminosity and k is a constant, set to match the data at $b_J=19.7$. So, for each spectrum we uniformly reduce the number of photons by the factor F appropriate to each magnitude giving our final estimated number of photons per pixel from the galaxy, P_g .

A similar procedure is used to calculate the number of photons from the sky for each pixel. We combined the Kitt peak sky spectrum (Kennicutt 1992) with a near-IR sky spectrum resulting in a spectrum with resolution 10 – 15Å as shown in figure A2. We normalised the spectrum so that the flux at 5500Å is unity, and scaled the spectrum to give a sky brightness of $B = 22.2$ per sq. arc sec., assuming that $B - V = 1.0$ (Smyth 1982). Multiplying by the response as a function of wavelength and scaling by the area of sky covered by a fibre finally gives the number of photons received from the sky for each pixel, P_s .

Noise in the spectra is simulated by adding a random deviate to the predicted number of photons per pixel. Assuming that there are no systematic errors, the expected variance in the observed number of photons per pixel is simply given by the Poisson error. So, for a pixel with both galaxy and sky, the total number of photons is $N_p = P_g + P_s$, and the $\text{var}(N_p) = P_g + P_s$. To estimate the number of galaxy photons, N_g , we must subtract an estimate of the sky photons N_s . If a single sky fibre is used to estimate the sky, then $\text{var}(N_s) = P_s$, and so the variance in the estimated number of galaxy photons in a pixel, N_g , is

$$\text{var}(N_g) = \text{var}(N_p - N_s) = P_g + 2P_s. \quad (\text{A2})$$

In practice more than one sky fibre can be used, so the variance in the subtracted sky spectrum could be reduced to P_s/n for n sky fibres. However, there are other systematic errors, such as variations in fibre throughput or scattered light, which will not decrease as more sky fibres are used. Such effects are impossible to quantify until full commissioning of the 2dF system takes place, so for this simulation we have altered equation (A2) to

$$\text{var}(N_g) = P_g + 1.5P_s. \quad (\text{A3})$$

to give an approximation of these factors. In practice this uncertainty affects the relation between magnitude and signal-to-noise by only a few tenths of a magnitude. CCD readnoise could be included in these calculations, but for 1800s exposures, the sky noise vastly dominates the readnoise, so it is irrelevant for the purpose of this investigation. So, for each pixel a random deviation is selected from a Poisson distribution with mean $P_g + 1.5P_s$, and this deviation is added to the predicted number of galaxy photons per pixel. The combination of sky lines and the response function leads to a large variation in signal to noise as function of wavelength along the spectrum.

Finally to produce the simulated reduced spectrum, the response function is divided out, and the spectrum fluxed,

de-redshifting to $z=0$ (this assumes that the redshift of the spectrum is derived by some other method), resampled to 4\AA bins, and normalized so that the average flux over the entire wavelength range is unity. Given the available wavelength range of the Normal26 spectra, this results in 768 bins covering the spectrum between 3712\AA and 6780\AA , which includes the strongest optical emission lines.

APPENDIX B: PRINCIPAL COMPONENT ANALYSIS

A pattern can be thought of as being characterized by a point in an M -dimensional parameter space. One may wish a more compact data description, where each pattern is described by M' quantities, with $M' \ll M$. This can be accomplished by Principal Component Analysis (PCA), a well known statistical tool, commonly used in Astronomy (e.g. Murtagh & Heck 1987 and references therein). The PCA method is also known in the literature as Karhunen-Loève or Hotelling transform, and is closely related to the technique of Singular Value Decomposition. By identifying the *linear* combination of input parameters with maximum variance, PCA finds M' variables (principal components) that can be most effectively used to characterize the inputs.

The first principal component is taken to be along the direction in the M -dimensional input parameter space with the maximum variance. More generally, the k th component is taken along the maximum variance direction in the subspace perpendicular to the subspace spanned by the first $(k-1)$ principal components.

The formulation of standard PCA is as follows. Consider a set of N objects ($i = 1, N$), each with M parameters ($j = 1, M$). If r_{ij} are the original measurements, we construct normalized properties as follows:

$$X_{ij} = r_{ij} - \bar{r}_j, \quad (B1)$$

where $\bar{r}_j = \frac{1}{N} \sum_{i=1}^N r_{ij}$ is the mean. We then construct a covariance matrix

$$C_{jk} = \frac{1}{N} \sum_{i=1}^N X_{ij} X_{ik}. \quad 1 \leq j \leq M \quad 1 \leq k \leq M \quad (B2)$$

It can be shown that the axis along which the variance is maximal is the eigenvector \mathbf{e}_1 of the matrix equation

$$C\mathbf{e}_1 = \lambda_1 \mathbf{e}_1, \quad (B3)$$

where the λ_1 is the largest eigenvalue, which is in fact the variance along the new axis. The other principal axes and eigenvectors obey similar equations. It is convenient to sort them in decreasing order, and to quantify the fractional variance by $\lambda_\alpha / \sum_\alpha \lambda_\alpha$. It is also convenient to re-normalize each component by $\sqrt{\lambda_\alpha}$, to give unit-variance along the new axis. We note that the weakness of PCA is that it assumes linearity and also depends on the way the variables are scaled. The matrix of all the eigenvectors forms a new set of orthogonal axes which are ideally suited to a description of the data set. A truncated eigenvector matrix using only ‘P’ eigenvectors

$$U_P = \{e_{jk}\} \quad 1 \leq k \leq P \quad 1 \leq j \leq M \quad (B4)$$

can be constructed where e_{jk} is the j th component of the k th eigenvector.

Now if we take a specific spectrum from the matrix defined in equation (B1), or possibly a spectrum from a different source which has been similarly normalized and mean subtracted, it can be represented by the vector of fluxes \mathbf{x} . We can find the projection vector \mathbf{z} onto the M principal components from

$$\mathbf{z} = \mathbf{x}U_M. \quad (B5)$$

Multiplying by the inverse, the spectrum is given by

$$\mathbf{x} = \mathbf{z}U_M^{-1} = \mathbf{z}U_M^\dagger, \quad (B6)$$

since U_M is an orthogonal matrix by definition. However, if we were to use only P principal components the reconstructed spectrum would be

$$\mathbf{x}_{rec} = \mathbf{z}U_P^\dagger, \quad (B7)$$

which is an approximation of the true spectrum.

APPENDIX C: ARTIFICIAL NEURAL NETWORKS

It is common in Astronomy and other fields to fit a model with several free parameters to observations. This regression is usually done by means of χ^2 minimization. A simple example of a model is a polynomial with the coefficients as the free parameters. Consider now the specific problem of morphological classification of galaxies. If the type of the i th galaxy is T_i (e.g. on the numerical system $[-5, 10]$), and we have a set of parameters \mathbf{x}_i (e.g. isophotal diameters, colours or spectral lines) then we would like to find the free parameters \mathbf{w} (‘weights’) such that the cost function

$$E = \frac{1}{2} \sum_{i=1}^N [T_i - F(\mathbf{w}, \mathbf{x}_i)]^2, \quad (C1)$$

is minimized. The non-linear function $F(\mathbf{w}, \mathbf{x})$ represents the ‘network’, which consists of a set of input nodes, a set of output nodes and one or more further layers of ‘hidden’ nodes between the input and output layers. The ‘hidden-layers’ allow curved boundaries around clouds of data points in the parameter space.

For a given network architecture the first step is the ‘training’ of the ANN. In this step the weights w_{ij} ’s (the ‘free parameters’) are determined by minimizing ‘least-squares’. Each node (except the input nodes) receives the output of all nodes in the previous layer and produces its own output, which then feeds the nodes in the next layer. A node at layer s calculates a linear combination over the n inputs $x_i^{(s-1)}$ from the previous layer $s-1$ according to

$$I_j^{(s)} = \sum_{i=0}^n w_{ij}^{(s)} x_i^{(s-1)} \quad (C2)$$

where the w_{ij} ’s are the weights associated with that node. Commonly one takes $x_0 = 1$, with w_{0j} playing the role of a ‘bias’ or DC level. The node then fires a signal

$$x_j^{(s)} = f(z), \quad (C3)$$

where z here stands for $I_j^{(s)}$, and f is a non-linear transfer function usually of the sigmoid form

$$f(z) = 1/[1 + \exp(-z)] \quad (C4)$$

in the interval $[0,1]$, or

$$f(z) = \tanh(z) \quad (C5)$$

in the interval $[-1,1]$.

For each galaxy in the training set, the network compares the output F with the desired type T to give a cost function (equation C1) averaged over all the training galaxies. This is minimized with respect to free parameters, the weights w_{ij} .

The interpretation of the network output depends on the network configuration. For example, a single output node provides a continuous output while several output nodes can be used to assign probabilities to different classes (e.g. 5 morphological types of galaxies, e.g. Storrie-Lombardi et al. 1992; Lahav et al. 1996). There are various optimization algorithms for finding the weights. One popular algorithm is the Backpropagation (e.g. Rumelhart, Hinton & Williams 1986; Hertz et al. 1991), where the minimization is done by the chain rule (gradient descent).

A more efficient method, used in our study, is Quasi-Newton. In short, the cost function $E(\mathbf{w})$ in terms of the weights vector \mathbf{w} is expanded about a current value \mathbf{w}_0 :

$$E(\mathbf{w}) = E(\mathbf{w}_0) + (\mathbf{w} - \mathbf{w}_0) \cdot \nabla E(\mathbf{w}_0) + \frac{1}{2} (\mathbf{w} - \mathbf{w}_0) \cdot \mathbf{H} \cdot (\mathbf{w} - \mathbf{w}_0) + \dots, \quad (C6)$$

where \mathbf{H} is the Hessian with elements $H_{ij} = \frac{\partial^2 E}{\partial w_i \partial w_j}$ evaluated at \mathbf{w}_0 . The minimum approximately occurs at

$$\nabla E(\mathbf{w}) \approx \nabla E(\mathbf{w}_0) + \mathbf{H} \cdot (\mathbf{w} - \mathbf{w}_0) = 0. \quad (C7)$$

Hence an estimation for the optimal weights vector is at

$$\mathbf{w} = \mathbf{w}_0 - \mathbf{H}^{-1} \nabla E(\mathbf{w}_0). \quad (C8)$$

In the standard Newton's method a previous estimate of \mathbf{w} is used as the new \mathbf{w}_0 . Calculating the Hessian exactly is expensive computationally, and in the quasi-Newton method an iterative approximation is used for the inverse of the Hessian (e.g. Press et al. 1992; Hertz et al. 1991).

The determination of many free parameters, the weights w_i 's in our case, might be unstable. It is therefore convenient to regularise the weights, e.g. by preventing them from growing too much. In the ANN literature this is called 'weight decay'. This approach is analogous to Maximum Entropy, and can be justified by Bayesian arguments, with the regularising function acting as the prior in the weight space. One possibility is to add a quadratic prior to the cost function and to minimize

$$E_{tot} = \alpha E_w + \beta E_D, \quad (C9)$$

where E_D is our usual cost function, based on the data (e.g. equation C1) and

$$E_w = \frac{1}{2} \sum_{i=1}^Q w_i^2 \quad (C10)$$

is the chosen regularising function, where Q is the total number of weights. The coefficients α and β can be viewed

as 'Lagrange multipliers'. While sometime they are specified ad-hoc, it is possible to evaluate them 'objectively' by Bayesian arguments in the weight-space. Approximately $\alpha^{-1} \approx 2\hat{E}_w/Q$ and $\beta^{-1} \approx 2\hat{E}_D/N$, (e.g. MacKay 1992, Ripley 1993, Lahav et al. 1996). We note that this analysis makes sense if the input and output are properly scaled e.g. between $[0, 1]$ with sigmoid transfer functions, so all the weights are treated in the regularisation process on 'equal footing'. It can be generalized for several regularising functions, e.g. one per layer.

We note that the addition of the regularisation term E_w changes the location of the minimum, now satisfying

$$\nabla E_D = -\frac{\alpha}{\beta} \nabla E_w = -\frac{\alpha}{\beta} \mathbf{w}, \quad (C11)$$

as from equation (C10) $\nabla E_w = \mathbf{w}$. The effect of the regularisation term here is reminiscent of the restoring force of an harmonic oscillator: the larger \mathbf{w} is the more it will get suppressed. We applied least-square minimization using a Quasi-Newton method as implemented in a code kindly provided to us by B.D. Ripley.

This paper has been produced using the Blackwell Scientific Publications L^AT_EX style file.